An Event-Related Potential-Based Adaptive Model for Telepresence Control of Humanoid Robot Motion in an Environment Cluttered With Obstacles

Mengfan Li, Wei Li, *Member, IEEE*, Linwei Niu, *Member, IEEE*, Huihui Zhou, Genshe Chen, *Member, IEEE*, and Feng Duan

***Abstract*—This paper develops an event-related potential (ERP)-based adaptive model for the control of humanoid robot movements in an environment cluttered with obstacles based on live video feedback. This model adaptively determines the repetition number according to an individual's mental state to speed up the robot control cycle. N200 and P300 potential features increase in the frontal and occipital areas when using robot images as visual stimuli, so it is able to effectively recognize target visual stimuli by processing Fisher's linear discriminant analysis (FLDA) and to identify a subject's intention by using support vector machine (SVM), in parallel. The offline evaluations show that, compared with a nonadaptive model, the adaptive model increases the accuracy rate from 88.8% to 92.9%, a change of 4.1%, and the information transfer rate (ITR) from 41.3 to 46.3 bits/min, a change of 5.0 bits/min. Eight subjects participated in telepresence controlling a NAO humanoid robot to move in an office environment cluttered with obstacles. The successful maneuvers demonstrate that the brain-controlled humanoid robot can be applied for surveillance and exploration in unknown environments based on live video feedback, which are evaluated by using new metrics for the performance of the brain–robot interaction (BRI) system.**

***Index Terms*—Brain–robot interaction (BRI), event-related potential (ERP)-based adaptive model, live video feedback, N200 and P300 potentials, telepresence control of humanoid robot.**

I. Introduction

A SYSTEM controlled via brain signals could assist healthy people or people with severe motor disabilities to accomplish tasks in special environments or daily life by establishing a direct connection between the brain and external devices [1]–[3]. It has shown potential applications in many fields: rehabilitation [1], [2], games [4], and military [5]. Event-related potential (ERP) is a type of brain signal defined as an electrical response of the cortex to stimuli. It includes N200 potential that is a negative valley appearing at poststimulus 180–325 ms and P300 potential that is a positive peak appearing at poststimulus 250–800 ms [6]. Since the first P300 speller based on the "oddball" paradigm was developed [7], the ERP-based brain–computer interface (BCI) systems have emerged, e.g., spelling sentences [8], controlling electrical applications in a virtual [9] or a lab environment [10], browsing Internet websites [11], controlling a wheelchair [12], [13], a hospital-bed nursing system [14], a robotic arm [15], and a humanoid robot [16]–[19]. Nevertheless, the telepresence control of a humanoid robot [20]–[24] via brain signals to perform complex operational tasks is not only helpful for the disabilities addressed in biomedical engineering but also very important for operators controlling humanoid robots in military, astronautic, and industrial applications.

Most of the ERP-based BCI systems need to repeatedly activate a visual stimulus associated with a selected target before they are able to identify the selected target stimulus; while setting the repetition number, one has to consider the tradeoff between accuracy rate and control cycle time. Increasing the repetition number improves the accuracy rate but slows down the control cycle speed [25]. Usually, a system with a constant repetition number cannot ensure the quality of induced ERPs due to individual factors, such as concentration and experiment

Manuscript received October 18, 2015; revised January 19, 2016; accepted January 22, 2016. Date of publication March 4, 2016; date of current version January 10, 2017. This work was supported in part by the National Natural Science Foundation of China under Grant 61473207 and in part by the State Key Laboratory of Robotics at Shenyang Institute of Automation under Grant 2014-Z03. *(Corresponding author: Wei Li.)*

M. Li is with the School of Electrical Engineering and Automation, Tianjin University, Tianjin 300072, China (e-mail: shelldream@tju.edu.cn).

W. Li is with Shenyang Institute of Automation, Chinese Academy of Sciences, Shenyang 110016, China, and with the School of Electrical Engineering and Automation, Tianjin University, Tianjin 300072, China, and also with the Department of Computer and Electrical Engineering and Computer Science, California State University, Bakersfield, CA 93311 USA (e-mail: wli@csub.edu).

L. Niu is with the Department of Mathematics and Computer Science, West Virginia State University, Institute, WV 25112 USA (e-mail: lniu@wvstateu.edu).

H. Zhou is with the McGovern Institute for Brain Research, Massachusetts Institute of Technology, Cambridge, MA 02139 USA, and also with the Shenzhen Institute of Advanced Technology, Chinese Academy of Sciences, Shenzhen 518055, China (e-mail: zhouhuih@mit.edu).

G. Chen is with Intelligent Fusion Technology, Germantown, MD 20876 USA (e-mail: gchen@intfusiontech.com).

F. Duan is with the Department of Automation and Intelligence Science, College of Computer and Control Engineering, Nankai University, Tianjin 300071, China (e-mail: duanf@nankai.edu.cn).

Color versions of one or more of the figures in this paper are available online at http://ieeexplore.ieee.org.

Digital Object Identifier 10.1109/TIE.2016.2538740

duration. In order to cope with these issues, some researchers have proposed adaptive methods to improve the ERP-based BCI performance [26]. The work [11] proposed an adaptive system based on motion-onset visual evoked potentials. This system automatically increased the number of presentations beginning with one until the system detected acceptable N200 potentials from the latest three repetitions. The work [27] applied an adaptive P300-based BCI system with a 12×7 matrix. The work in [28] proposed an approach to improving speller performance by combining both N200 and P300 potentials.

Control of humanoid robots via brainwaves is challenging, because complex tasks and dynamic environments with uncertainty [29], [30] require subjects to output commands fast and accurately to ensure safe operations. The recent work [18] proposed a N200-based model for telepresence control of a NAO humanoid robot and confirmed that the repetition number in a trial significantly affects the performance of telepresence control of the NAO robot. A large repetition number increases the duration required to output a single command, leading to an increase in the total time to complete the operational task. On the other hand, the large number delivers a high accuracy rate, leading to a reduction in the number of incorrect commands in the control process, i.e., to avoid additional time to correct the false instructions. Optimizing the repetition number to improve the information transfer rate (ITR) is a key issue to minimizing the total time of completing an operational task. The previous experiments in [31] indicate that a desired repetition number depends highly on an individual subject and the mental state of the subject performing the experiment. Until now, only the studies presented herein and in [31] addressed the ERP-dominated adaptive models for telepresence control of a humanoid robot. In order to make the repetition number suitable for each subject in the ERP-based model, an ERP-based adaptive model is proposed by automatically setting the repetition number in a trial for telepresence control of the NAO humanoid robot with high degrees of freedom (DOF) using live video feedback.

The study [32] discovered that using a flashing robot image as visual stimuli can sequentially induce both N200 and P300 potentials with recognizable features, so this paper develops an adaptive model using both N200 and P300 potentials to improve accuracy rates and to speed up the control cycle by minimizing the iterative number of repetitions. The adaptive model uses both Fisher's linear discriminant analysis (FLDA) and a support vector machine (SVM) in parallel to recognize a target stimulus by comparing an input vector with trained patterns, and then fuses their classification results to detect a subject's intentions. The adaptive model is implemented on Cerebot—a mind-controlled humanoid robot platform [33]–[35] to evaluate its performance. A coordination mechanism is embodied in the brain-controlled system, so that subjects are able to flexibly select robot behaviors and execution modes according to the environments and the tasks.

Eight subjects participated in experiments controlling robot-walking behaviors. Both the offline and online evaluations reported average accuracy rates of 92.9% and 91.6%, average repetition numbers of 2.1 and 2.7, and average ITRs of 46.3 and 35.5 bits/min achieved by the adaptive model, respectively. The adaptive model was validated by using a complex teleoperation: controlling the humanoid robot to move into an environment

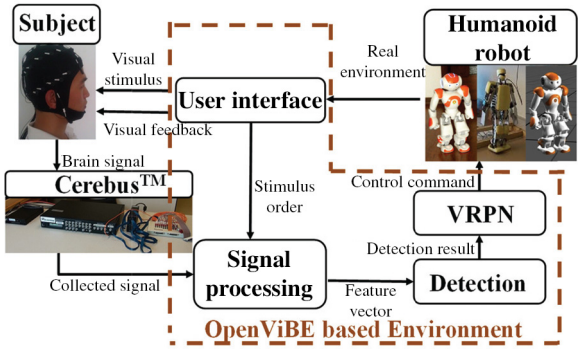

Fig. 1. Cerebot—a mind-controlled humanoid robot platform.

with obstacle avoidance using live video feedback. Compared to the model in [18], the adaptive model used a lower average repetition number to reach a higher ITR with an accuracy rate of over 90.0%. All the subjects successfully controlled the NAO robot to avoid obstacles in a narrow environment. The proposed adaptive model can be used to control the humanoid robot to perform a variety of complex tasks with full body movements, such as walking, picking up objects, or climbing, when the visual stimuli are adopted to encode the corresponding robot behaviors. Other than the traditional performance indices of a BCI system, the authors used new metrics to evaluate the performance of the brain–robot interaction (BRI) system.

This paper is organized as follows. Section II first introduces the mind-controlled humanoid robot platform, and then describes the protocol and procedure for acquiring the N200 and P300 potentials. Section III presents the combined classification algorithm and the adaptive model for controlling the humanoid robot, and depicts how the system provides two execution modes for a subject. Section IV analyzes the features of N200 and P300 potentials and evaluates the control performance of the proposed model. Section V compares the proposed model with the existing adaptive models. Section VI presents conclusion.

II. Acquiring N200 and P300 Potentials

A. Cerebot

The adaptive model was developed under the OpenViBE programming environment [36]. OpenViBE is an open-source software for conveniently reading, displaying, and processing brain signals, and provides user-friendly interfaces to scripts written in MATLAB, Python, or C++ via the Virtual-Reality Peripheral Network (VRPN). The adaptive model was implemented on Cerebot, consisting of a Cerebus Data Acquisition System, a humanoid robot NAO/KT-X PC, and a virtual NAO robot, as shown in Fig. 1. Cerebus collects brain signals induced by visual stimuli. Cerebot has integrated Webots, OpenGL, OpenCV, Choregraph, Central software, and user-developed modules in C++ and MATLAB.

B. Experimental Protocol

The experimental protocol addresses a method to present a 2×3 stimulus matrix on the user interface. The six images

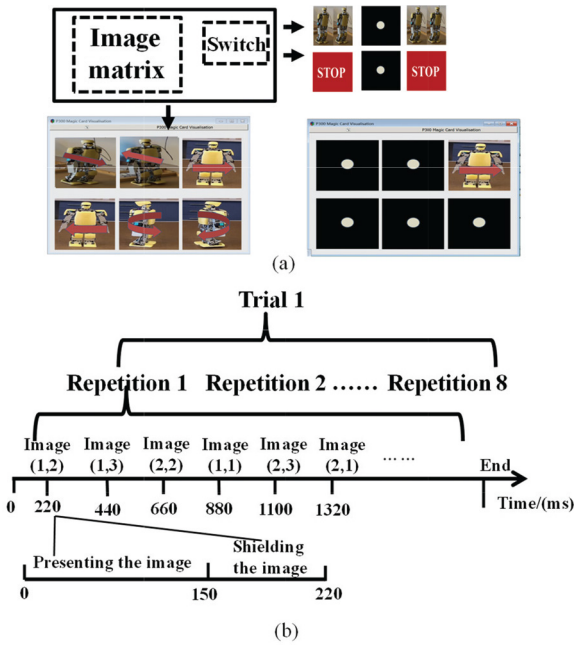

Fig. 2. (a) Robot image of shifting left located at row 1 and column 3 is presented and the remaining images are shielded. The images that represent the CW and SW are flashed on the right top corner. (b) Trial protocol consists of eight repetitions.

that are taken from a real robot to make the visual stimuli impressive and intuitive represent six robot-walking behaviors: walking forward, walking backward, shifting left, shifting right, turning left, and turning right, as shown in the second row of Fig. 2(a). A black square with a white solid circle is defined by the shielding image to shield the robot images. Activating a visual stimulus in the user interface is to switch the shielding image to its corresponding robot image.

This study adopts a single character (SC) method [37] to activate robot images as visual stimuli in a random order. The probability of presenting each stimulus is equal to 1/6 [7]. When one robot image is flashing, all the remaining robot images are shielded by the shielding image. A stimulus onset asynchrony (SOA), i.e., an interval between activating two visual stimuli, is 220 ms, including 150 ms of presenting a robot image and 70 ms of shielding the six robot images, as shown in Fig. 2(b). The process in which all six robot images are presented is defined as a "repetition." The visual stimuli are categorized into a target stimulus on which a subject has to focus and five nontarget stimuli that the subject should ignore. Several repetitions constitute a trial in which the subjects focus on one robot image as the target stimulus. Most of the P300-based models choose a constant number of repetitions for a trial [7], [37]. The adaptive model chooses a repetition number of 8 for calibration in the offline process.

C. Experimental Procedure

The experimental procedure displays the visual stimuli on a 21-in LCD monitor with a resolution of 1280×1024 pixels and uses a 32-channel EEG cap to acquire brain signals over the scalp. The channels are arranged according to the "International 10-20 system." Channel AFz is the ground electrode and the reference channels are the linked mastoids.

The eight subjects (1 female and 7 males) are right-handed, have normal or corrected-to-normal eyesight, and signed written informed consents to participate in the experiments. The majority of them had no prior experience on P300 or N200 experiments. The experimental procedure includes the offline training [11], [27], [28] and online control. The offline training stage allowed all subjects with different prior BRI experiences to become familiar with the experimental setup. They sat in a comfortable chair at a distance of 60 cm from the monitor and kept their eyes at the same horizontal level as the user interface center. Each subject conducted 48 trials (384 repetitions) to collect brain data for offline training of the patterns of N200 and P300 potentials.

III. Adaptive Control Model

A. Feature Representation

The adaptive model establishes a feature vector representing N200 and P300 potentials by the brain signals acquired from 13 channels {O2, O1, Oz, Pz, P4, P8, P3, P7, Cz, FCz, Fz, F4, F3} as follows. The first step is to cut the brain signals into epochs using a window from poststimulus 100 ms to poststimulus 500 ms. The second step is to eliminate a drift from the epochs by the common average reference (CAR) algorithm [38]. The next two steps are to process the epochs by a digital filter with a bandwidth of 1–10 Hz and to subtract the baseline from the epoch. The fifth step is to downsample the epochs from 1000 to 20 Hz, as shown in Fig. 3. Then, each epoch is transformed to a time series with eight elements $((500-100)/1000 \times 20 = 8)$. The elements are the brain signals at points of 100, 150, $\cdots$, 400, and 450 ms, which describe the shape of N200 and P300 potentials. Elements 3–5 in the time series from the channels located in the frontal and central areas represent N200 potentials; elements 3–7 from the channels located in the parietal and occipital areas, and elements 6–8 from the channels located in the frontal and central areas represent P300 potentials. The time series from each channel under the same visual stimulus is averaged several times to obtain a feature vector $(\overline{\boldsymbol{a}}_1^{\text{ch}}, \overline{\boldsymbol{a}}_2^{\text{ch}}, \ldots \overline{\boldsymbol{a}}_8^{\text{ch}})$. The last step is to use the brain signals acquired from the 13 channels to build a 13×8 matrix and to convert it into a 104-dimension feature vector. For a trial, one needs to build six feature vectors that are corresponding to the six visual stimuli.

B. Classification

1) Fisher's Linear Discriminant Analysis: An FLDA was used to calculate a d-dimension discriminant vector $\boldsymbol{w} \in R^d$ that groups the vectors with the same features into a class [39]. It classifies a feature vector by the following function:

$$f(\boldsymbol{x}) = \boldsymbol{w}^T \boldsymbol{x} - \boldsymbol{w}_0 \tag{1}$$

where w_0 is a threshold and $\boldsymbol{x}$ is the input vector. The feature vector belongs to the target class if $f(\boldsymbol{x})$ is positive.

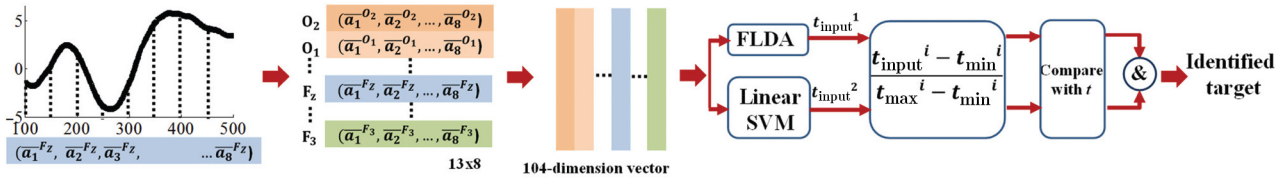

Fig. 3. Time series from poststimulus 100–500 ms is downsampled to 20 Hz. The combined classification algorithm classifies a 104-dimension feature vector that is established by the time series from 13 channels.

2) Support Vector Machine: SVM is a machine-learning algorithm based on statistical theory [40], [41]. The libSVM toolbox [42] with a linear kernel function accomplishes the classification

$$f(\boldsymbol{x}) = \sum_{i=1}^{n} \alpha_i^* y_i K(\boldsymbol{x}_i, \boldsymbol{x}) + b^* \tag{2}$$

$$K(\boldsymbol{x}_i, \boldsymbol{x}) = \boldsymbol{x}_i^T \boldsymbol{x} \tag{3}$$

where $\boldsymbol{x}_i$ belongs to a set of training vectors.

3) Combined Classification Algorithm: In general, a trained classifier transforms an input vector to a scalar value and judges the vector as a target if the value is larger than 0. The training phase trains the FLDA and linear SVM classifiers, separately. The inputs to the trained FLDA and SVM classifiers are the target and nontarget samples, and the outputs are the maximum value $t^i_{\max}$ and the minimum value $t^i_{\min}$, where $i = 1$ represents the FLDA and $i = 2$ represents the SVM. The absolute values of the maximum and minimum represent the largest distances between the hyperplane and the two classes. In the test phase, the FLDA and SVM classifiers transform an input vector to a scalar value t^i_{input} in parallel, where t^i_{input} is calculated by (1) or (2). Each classifier judges the input vector by comparing $t^i = \left(t^i_{\text{input}} - t^i_{\min}\right) / \left(t^i_{\max} - t^i_{\min}\right)$ with a threshold t (in this study, $t = 0.4$), as shown in Fig. 3. If t^i is larger than t, the single classifier labels the input vector as a target stimulus. When both the classifiers label the input vector as the target stimulus, the input vector is classified as the target. Otherwise, the vector is classified as the nontarget stimulus. The combined classification algorithm decreases the possibility of incorrectly classifying nontarget stimuli.

C. Adaptive Model

Increasing the repetition number n of a trial improves the accuracy rate of identifying a target stimulus, but decreases the online control speed. An ERP-based model with a constant repetition number may not work well with individual differences. The quality of N200 and P300 potentials of a subject indicates his/her mental activity strength. For example, if the subject concentrates on target stimuli well, only a few repetitions are able to produce N200 and P300 potentials with recognizable features; otherwise, more repetitions are needed to detect the features of N200 and P300 potentials. To tackle the problems, this study proposes an adaptive model that automatically adjusts the repetition number according to the subject's mental states. Fig. 4 shows the flow diagram of the adaptive model. The model is specified by its minimum repetitions $n_{\min}$

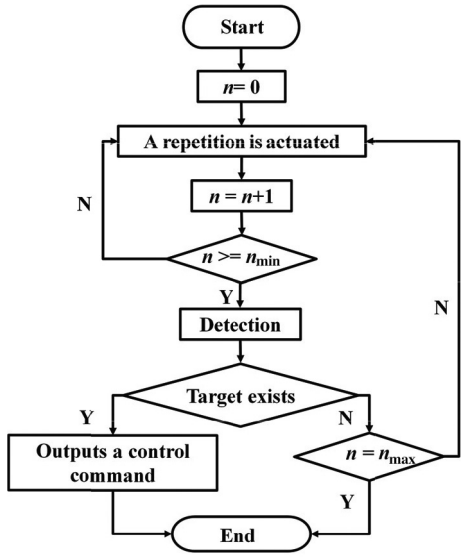

Fig. 4. Flow diagram of the adaptive algorithm.

and its maximum repetitions $n_{\max}$. It executes at least $n_{\min}$ repetitions to begin detection and increases the repetition by one until it detects a target stimulus. The model outputs a classification result and stops this trial if it detects a target stimulus with repetitions $n_{\min} \le n \le n_{\max}$. It fails if it is not able to detect the target stimulus at $n_{\max}$ repetitions and starts a new trial. Depending on the subject's mental state, the adaptive model varies the repetition number to accurately identify the subject's intention.

D. Execution Mode Switch

When executing a behavior, it is better for the robot to adjust the execution mode of this behavior based on the working task and environment. Step-by-step execution is suitable for tasks that require high finesse, e.g., walking through a curve in a narrow environment. While continuous execution is good for tasks that require high speed, e.g., a long-distance walking task. The proposed system provides two modes of robot walking for the subject: step walking (SW) mode and continuous walking (CW) mode. When the robot receives a control command, it walks for about 10 cm with fixed steps and then automatically stops in the SW mode. The robot, in the CW mode, keeps walking at a speed of about 5 cm/s and does not stop until it receives a stop command.

A switch visual stimulus, located at the right top corner of a monitor as seen in Fig. 2(a), switches the robot to the CW mode for the target-walking behavior. When one of the six robot images is detected as a target, the subject has 5000 ms to set

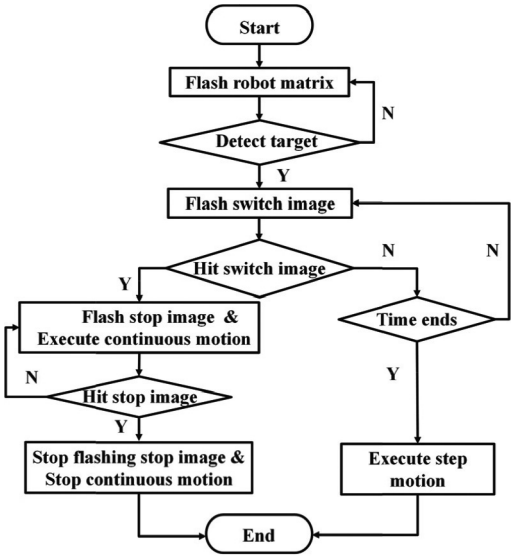

Fig. 5. Flow of selecting execution modes and beginning a new trial.

the execution mode of this target behavior as the CW mode by focusing on the switch visual stimulus. The system declares that the switch visual stimulus is hit if it detects the subject's ERPs during this time. In this case, the system activates the robot in the CW mode and changes the switch visual stimulus to the stop, one at the same time. If the switch visual stimulus is not hit, the robot acts in the SW mode during the next 5000 ms, and then a new trial begins. The subject could stop the CW mode and start a new trial by hitting the stop visual stimulus. Fig. 5 shows the flow of the switching. The CW, an alternative mode of controlling the robot, relieves the subject's work load by decreasing the command number when the subject needs to keep the robot acting in the same behavior for several repetitions.

IV. Performance Evaluation

A. Signal Analysis

This section discusses the features of the induced N200 and P300 potentials over the eight subjects as follows. First, a window from prestimulus 300 ms to poststimulus 1000 ms cuts brain signals into epochs. Second, a digital filter filters the epochs with a bandwidth of 1–10 Hz. Third, the baseline which is the mean value of an epoch from prestimulus 300–0 ms is subtracted from the epoch. Finally, an algorithm averages the epochs induced by the same type of stimuli, including target or nontarget stimuli. Fig. 6(a) shows that the interface sequentially evokes N200 and P300 potentials in channels Fz, Cz, and Oz. The solid and dashed curves in Fig. 6(a) represent the average brain signals induced by the target and nontarget stimuli, respectively. The positive peak of P300 potentials from channel Oz appears at about 230 ms and from channels Fz and Cz appear at about 370 ms, and their amplitudes range from 3 to 6 μV. N200 potentials are mainly induced in the frontal and central areas, e.g., Fz, F3, F4, and Cz, and their sharp negative valleys reach 4 μV at about 260 ms. The differences between the brain signals produced by the target stimuli and nontarget

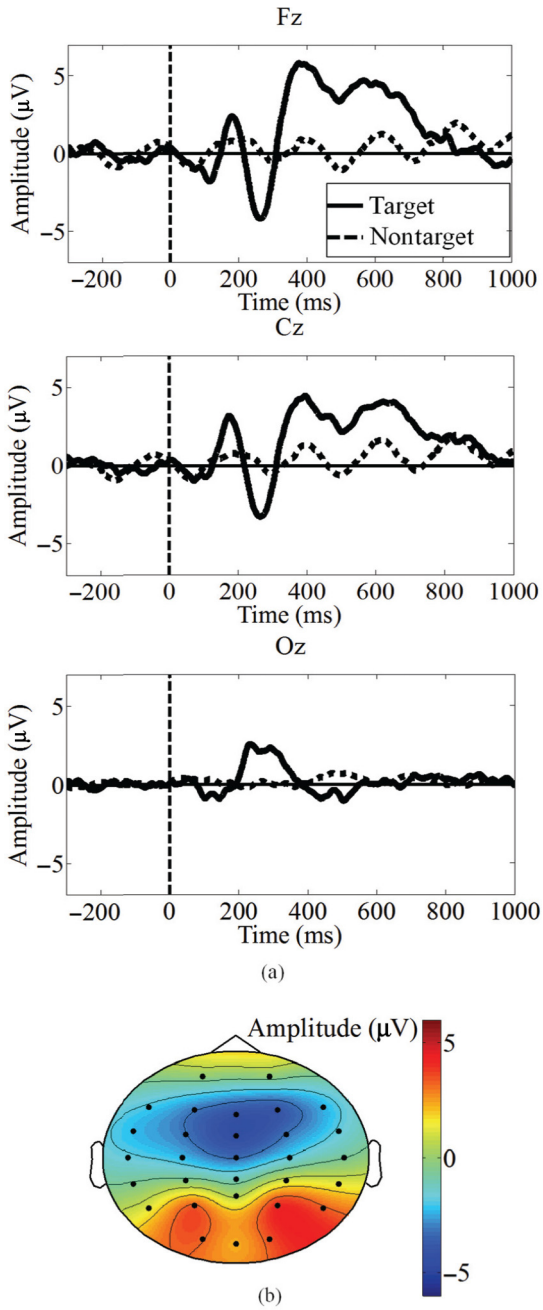

Fig. 6. (a) Average N200 and P300 potentials from channels Fz, Cz, and Oz. The dashed vertical lines indicate the start time of stimuli. (b) Topographic map of evoked potentials at poststimulus 260 ms.

stimuli mainly occur from poststimulus 200–800 ms. Fig. 6(b) depicts the topographic map of the evoked potentials at poststimulus 260 ms. N200 potentials appear clearly in the middle line of the frontal and central areas and decrease in the two sides of the scalp. The P300 potentials show large amplitudes in the occipital and parts of the parietal areas, especially in the two sides of these areas.

B. Comparison of Classifiers

The true positive ratio (TPR), the false positive ratio (FPR) [43], and the Youden's index are used to measure the FLDA

TABLE I
COMPARISON OF THE CLASSIFIERS

Methods	TPR (%)	TNR (%)	Youden's index
FLDA	**95.0**	67.5	0.625
SVM	82.5	**97.8**	0.803
Combined	91.3	90.5	**0.818**

and SVM's sensitivity, specificity, and comprehensive ability on discriminating the target and nontarget samples

$$\text{TPR} = \frac{\text{TP}}{\text{TP} + \text{FN}} \times 100\% \tag{4}$$

$$\text{TNR} = \frac{\text{TN}}{\text{TN} + \text{FP}} \times 100\% \tag{5}$$

$$\text{Younden}'\text{s index} = \text{TPR} + \text{TNR} - 1. \tag{6}$$

The samples are divided for training and testing a classifier. A trained classifier labels every test sample as a target or nontarget sample. TP stands for the target sample that is correctly classified as a target, FN stands for the target sample that is classified incorrectly as a nontarget, TN stands for the nontarget sample that is correctly classified as a nontarget, and FP stands for the nontarget sample that is incorrectly classified as a target. Table I shows the TPR, TNR, and Youden's index of the three classifiers when the repetition number is 2. The higher these three indices are, the better the corresponding classifier. The FLDA reaches the highest TPR and the lowest TNR, while the SVM reaches the lowest TPR and the highest TNR. The combined classification algorithm shows relatively high performances on both TPR and TNR, and reaches the highest level of Youden's index. The computing time cost of these classifiers is in the order of 10 ms, so their impacts on controlling humanoid robot-walking behavior with dynamic responses in the order of seconds can be ignored. Therefore, the combined classification algorithm was chosen as the classifier to detect the target stimuli in the adaptive model. When failing to detect a target stimulus in the first n repetitions, the proposed adaptive model starts a new repetition to detect the target, so the combined classification algorithm's chance of missing the target stimuli is decreased.

C. Nonadaptive Model

This study begins the performance evaluation with a nonadaptive model, which was used to control a robot system [12], [15], [16]. Assessing the classification accuracy rate uses the 10-fold cross-validation [11] method. Fig. 7(a) represents the accuracy rates of the three classifiers versus the repetition number n. When n increases from 1 to 8, the accuracy rates rise from about 70.0% to above 95.0%. The accuracy rate yielded by the combined classification algorithm is slightly higher than the rates of the FLDA and the SVM. Although both the FLDA and combined classification algorithms yield similar ITRs, i.e., the close accuracy rates, the combined algorithm is useful to detect the idle mental state, i.e., to reduce classification mistakes when no visual stimulus is selected as a target. The idle mental state keeps the robot walking without the need for outputting any commands from the CW mode.

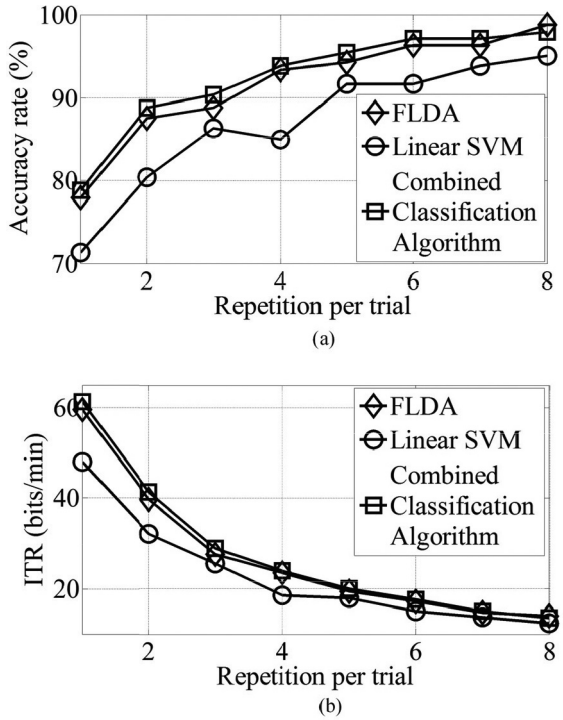

Fig. 7. Curves represent the (a) average accuracy rates and (b) ITRs when the repetition number n ranges from 1 to 8.

ITR is considered as an important performance measure for the BCI system. One uses ITR to assess the control cycle speed described in [1]

$$B = \left[\log_2 N + \log_2 P + (1-P) \times \log_2 \left(\frac{1-P}{N-1}\right)\right] \times M \tag{7}$$

where P is the accuracy rate, $N = 6$ is the candidate number of visual stimuli, and M is the number of outputting commands per minute. Fig. 7(b) shows that ITRs decrease as n increases. This is because a larger repetition number leads to a longer duration of outputting a command, and then M becomes smaller and decreases the B. Fig. 7 shows that the repetition number is important for balancing the accuracy rate and control cycle speed of the BRI system.

D. Offline Evaluation of Adaptive Model

The offline evaluation means that the brain signals are recorded during the experiments and processed after the experiments. The adaptive model sets $n_{\min} = 2$ and $n_{\max} = 8$ based on the offline evaluation result of the nonadaptive model. As discussed above, the adaptive model automatically increases the repetition number until the model detects recognizable features of N200 and P300 potentials. Eight subjects participated in the experiments for this evaluation. Table II lists the offline evaluation results yielded by the adaptive model. The adaptive model usually detects the features of N200 and P300 potentials with two or three repetitions. The average repetition number is 2.1. Most of their accuracy rates are above 90.0%, and two of the eight subjects reached accuracy rates of 100.0%. All

TABLE II
SUBJECTS' PERFORMANCE

Subj	Offline (online) $\bar{n}$	Offline (online) Accuracy rate (%)	Offline (online) ITR (bits/min)
S1	2.1 (2.4)	96.7 (96.7)	49.7 (43.5)
S2	2.0 (2.1)	100.0 (100.0)	58.7 (55.9)
S3	2.1 (2.7)	96.7 (80.6)	49.7 (24.0)
S4	2.1 (2.4)	100.0 (100.0)	55.9 (48.9)
S5	2.1 (2.9)	90.0 (81.8)	40.8 (22.4)
S6	2.1 (2.1)	76.7 (89.6)	27.3 (40.3)
S7	2.1 (3.3)	96.7 (88.1)	49.7 (24.6)
S8	2.0 (4.1)	86.7 (95.6)	38.8 (24.7)
Mean	2.1 (2.7)	92.9 (91.6)	46.3 (35.5)

Online accuracy rates are in parentheses.

of the subjects achieved average ITRs over 25.0 bits/min, and their overall average ITR reached 46.3 bits/min. S4, who for the first time participated in this kind of experiment, delivered the desired performance with an accuracy rate of 100.0% and an ITR of 55.9 bits/min. Compared with the nonadaptive model with $n = 2.0$, the adaptive model increases the average accuracy rate from 88.8% to 92.9% and the average ITR from 41.3 to 46.3 bits/min. The adaptive model uses about two repetitions to achieve the accuracy rate, which is approximately equivalent to the one yielded by the nonadaptive model with $n = 4.0$; however, it reduces the trial time to half. The results in Table II demonstrate that the adaptive model improves the control cycle speed with a high accuracy rate, which then shortens the total time needed for completing the tasks. All the participants improved their accuracy rates and ITRs with the adaptive model, so comparative studies would be conclusive and significant.

E. Online Evaluation of the Adaptive Model

The online evaluation means that the brain signals are acquired and processed synchronously during the experiments, and the NAO humanoid walking behavior is controlled in open loop with the adaptive model. One still takes $n_{\min} = 2$ and $n_{\max} = 8$.

Table II lists the online evaluation results of open-loop control of the NAO humanoid robot. The eight subjects participated in the online evaluation. S2 achieved the best performance with an average repetition number of 2.1, an average accuracy rate of 100.0%, and an average ITR of 55.9 bits/min. S7 and S8 needed more than three repetitions. Their overall average repetition number is 2.7. Compared with the nonadaptive model with $n = 3$, the adaptive model increases the average accuracy rate from 90.4% to 91.6% and the average ITR from 28.9 to 35.5 bits/min.

F. Telepresence Control of the NAO Robot

An experiment of telepresence control of the NAO to move in an environment requiring obstacle avoidance was conducted to test the feasibility of the adaptive model. The subjects needed to focus on a target stimulus and a video clip to control the robot to move to a destination bypassing the environment cluttered with

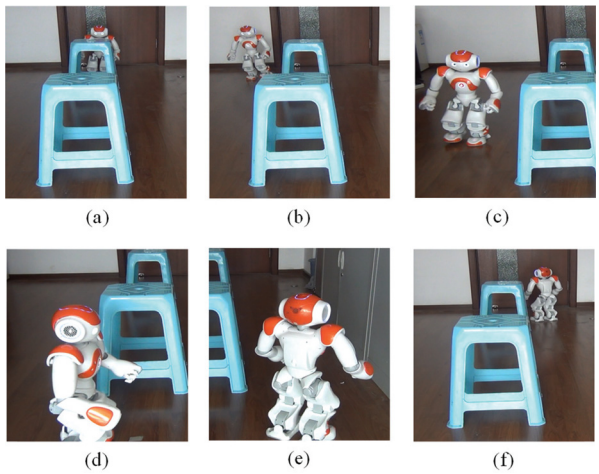

Fig. 8. Snapshots of the obstacle avoidance experiment. (a) Walk forward. (b) Shift right. (c) Walk forward. (d) Turn left. (e) Turn left. (f) Walk forward.

TABLE III
ROBOT CONTROL PERFORMANCE

Subj	Total time (s)	Total CMDs	No. of SW	No. of CW	Ave* $\bar{n}$	Suc ** (%)
S1	504.3	76.7	14.7	20.7	2.9	90.9
S2	393.3	44.0	10.0	11.3	3.0	96.9
S3	943.0	74.0	38.0	12.0	2.5	82.0
S4	722.5	77.0	41.0	12.0	2.5	93.5
S5	805.0	61.5	55.5	2.0	2.1	88.0
S6	407.3	52.7	8.7	14.7	3.2	90.8
S7	487.5	67.5	13.5	18.0	2.9	84.6
S8	410.7	48.0	14.0	11.3	2.7	88.6
Mean	584.2	62.7	24.4	12.8	2.7	89.4

Ave* stands for the average repetition number.
Suc** stands for the success rate.

obstacles. A series of video clips in Fig. 8 display the entire walking process of the humanoid robot in the environment. Images in Fig. 8(a) and (b) show that a subject controls the robot to avoid an obstacle by shifting right. Fig. 8(c) shows that the subject activates the walking-forward behavior again when the robot is on a collision-free path. Fig. 8(d) shows that the subject controls the robot to reach a destination. Fig. 8(e) and (f) shows that the robot turns left and walks on a collision-free path to return to the starting point. Table III lists each subject's performance on total time, total commands (CMDs), the number for each kind of command, success rate, and average repetitions. The commands include SW, CW, CW start, and CW stop commands. The first two represent the execution mode of the selected behavior; the latter two mean the subject switches to the CW mode and stops. Note that the numbers of the last three should be the same. The subject S2 spent 393.3 s finishing the task by 10.0 CW steps and 11.3 step-by-step walking steps with the highest success rate of 96.9%. On average, the eight subjects spent 584.2 s to generate 62.7 commands to complete the task. For the telepresence control, the adaptive model reaches an average success rate of approximately 90.0% with 2.7 repetitions.

TABLE IV
COMPARISON OF THE ADAPTIVE MODEL

Evaluation type	N200 model [11]	P300 model [27]	N200 and P300 model [28]	N200 and P300 model proposed
Offline Nonadaptive	N/A	N/A	Acc: 60.0% ITR_T: 39.0 n=1	Acc: 78.8% ITR_T: 44.4 n=1
Offline Adaptive	ITR_R: 27.0	N/A	N/A	Acc: 92.9% ITR_R: 33.6 $\overline{n}$=2.1
Online Adaptive	Acc: 83.0% ITR_R: 42.1 $\overline{n}$=2.3	Acc: 98.0% ITR: 38.7 $\overline{n}$=4.6	Acc: 96.0% ITR_T: 35.6 $\overline{n}$=2.7	Acc: 91.6% ITR: 35.5 ITR_T: 30.9 ITR_R: 25.8 $\overline{n}$=2.7
Application	Output 15.1 commands to open Wikipedia;	Output 5 character -s;	N/A	Output 62.7 commands to control the NAO with obstacle avoidance;
	Time: 119.1 s; Suc: 91.0% $\overline{n}$=4.1	ITR: 44.2		Time: 584.2 s; Suc: 89.4% $\overline{n}$=2.7

Acc and Suc represent accuracy rate (%) and success rate (%), respectively. The unit of ITR is bits/min.

V. DISCUSSION

A. Comparison With the Existing Adaptive Models

The nonadaptive model yields an average ITR of 61.2 bits/min when the repetition number is $n = 1$, but an average accuracy rate below 80%. When the nonadaptive model increases its repetition number to 6 or 7, it achieves its average accuracy rate above 97.0%, but dramatically decreases its average ITR below 15.0 bits/min. Therefore, it is very difficult to create a balance between a high accuracy rate and a fast ITR with the nonadaptive model. The proposed adaptive model achieves an average accuracy rate of above 90.0%, and an average ITR of 46.3 bits/min in the offline evaluation and that of 35.5 bits/min in the online evaluation when the average repetition number is $2 < \overline{n} < 3$, so the adaptive model is much more efficient.

Next, the performance achieved by the proposed model was compared with the ones reported in [11], [27], and [28]. These references define the different ITR concepts, including the ITR with an interval between two trials denoted as ITR_T [28], the ITR with the interval between two repetitions denoted as ITR_R [11], and the ITR without considering any interval [27], so ITR_T and ITR_R of the proposed adaptive model are also listed in Table IV.

1) The offline evaluation studies on the nonadaptive model [28] document an accuracy rate of 60.0% and an ITR_T of 39.0 bits/min when $n = 1$, while the nonadaptive model proposed herein achieves an accuracy rate of 78.8% and an ITR_T of 44.4 bits/min when $n = 1$.
2) The offline evaluation studies on the adaptive model [11] document an ITR_R of 27.0 bits/min, while the proposed adaptive model reaches an ITR_R of 33.6 bits/min and an accuracy rate of 92.9% with $\overline{n} = 2.1$.
3) The adaptive model [27] uses $\overline{n} = 4.6$ to reach an ITR of 38.7 bits/min and an accuracy rate of 98.0%. The model [28] presents an ITR_T of 35.6 bits/min and an accuracy rate of 96.0% when $\overline{n} = 2.7$, but the reported experiments are not based on controlling a humanoid robot with dynamics. The model [11] achieves an accuracy rate of 83.0% and an ITR_R of 42.1 bits/min when $\overline{n} = 2.3$.
   For open-loop control of the NAO robot-walking behavior, the proposed adaptive model achieves an accuracy rate of 91.6%, an ITR_R of 25.8 bits/min, an ITR_T of 30.9 bits/min, and an ITR of 35.5 bits/min when $\overline{n} = 2.7$, respectively. Note that the higher accuracy rate would be a priority for dynamically controlling the humanoid robot safely.
4) Table IV lists the application cases. The model [11] outputs an average of 15.1 commands within 119.1 s to open Wikipedia using the Google browser and records a success rate of 91.0% and $\overline{n} = 4.1/\texttt{command}$. The proposed adaptive model outputs an average of 62.7 commands within 584.2 s to control the NAO robot to walk from an initial location to a destination with obstacle avoidance in the office environment and records a success rate of 89.4% and $\overline{n} = 2.7/\texttt{command}$. Model [27] outputs five characters on the screen with an ITR of 44.2 bits/min, but does not report the response time, the repetition number, and the success rate for the application.

B. Impacts of Execution Modes on Performance

First, CW increases the control speed. In Table III, although S1 and S4 use almost an equal amount of command numbers to accomplish the task, S1, who outputs more commands with CW, spends 208.2 s less than S4. This is because CW enables the robot to walk continuously and reduces the subject's time of selecting the same behavior for several instances. Second, executing in SW may be faster when the robot needs to act a specific behavior in a small range. If the behavior is executed in a large range and cannot be stopped in a certain timely manner, it may waste the subject's time to modify this, e.g., S3 uses fewer commands than S4 but finishes the work with more time left. The reason for this is that S3 gives the wrong commands in CW and sometimes cannot stop it in a timely manner, which leads to utilizing more time. Third, the subjects noted that adding CW to the system reduces their fatigue by decreasing the number of commands, but it might increase the difficulty of completing the task because they need to think about which mode is suitable and switch their attention as fast as possible when a target is hit. Fourth, as the robot control experiment adopts the visual feedback and mode switching, the subject's attention and state might be negatively affected, and the success rate may decrease slightly.

VI. Conclusion

This paper has developed an adaptive model by combining N200 and P300 potentials. The study in [32] shows that the designed user interface is able to sequentially induce N200 and P300 potentials by flashing images representing robot walking behavior, which allows one straightforwardly to establish their feature patterns. Different from the reports in [11] and [28], the N200 potentials induced by the adaptive model mainly appear in the frontal and central areas of the brain. This adaptive model automatically changes the repetition number in a trial based on the subjects' mental state. Compared to the nonadaptive model, the proposed adaptive model increases the accuracy rate and ITR, respectively, by 4.1% and 5.0 bits/min. It should also be noted that the assessment of the performance of BCI and BRI systems may be different. The telepresence control of the NAO robot via brainwaves is much more difficult and challenging, because one has to consider the impact of the robot dynamics and live video feedback on the subjects. The BCI systems proposed in [11], [27], and [28] were not validated by controlling a humanoid robot with high DOFs. Nevertheless, the proposed adaptive model successfully controlled the NAO humanoid robot to move in the environment cluttered with obstacles.

References

[1] J. R. Wolpaw, N. Birbaumer, W. J. Heetderks, D. J. McFarland, P. Hunter Peckham, and G. Schalk, "Brain–computer interface technology: A review of the first international meeting," *IEEE Trans. Rehabil. Eng.*, vol. 8, no. 2, pp. 164–173, Jun. 2000.

[2] M. A. Lebedev and M. A. Nicolelis, "Brain–machine interfaces: Past, present and future," *Trends Neruosci.*, vol. 29, no. 9, pp. 536–546, Jul. 2006.

[3] A. Ortiz-Rosario and H. Adeli, "Brain–computer interface technologies: From signal to action," *Rev. Neurosci.*, vol. 24, no. 5, pp. 537–552, Oct. 2013.

[4] B. J. Lance, S. E. Kerick, A. J. Ries, K. S. Oie, and K. McDowell, "Brain–computer interface technologies in the coming decades," *Proc. IEEE*, vol. 100, Special Centennial Issue, pp. 1585–1599, May 2012.

[5] B. Allison, B. Graimann, and A. Gräser, "Why use a BCI if you are healthy," in *Proc. Adv. Comput. Entertain. Technol., Workshop-Brain-Comput. Interfaces Games, Austry*, Jun. 13–15, 2007, pp. 7–11.

[6] S. H. Patel and P. N. Azzam, "Characterization of N200 and P300: Selected studies of the event-related potentials," *Int. J. Med. Sci.*, vol. 2, no. 4, pp. 147–154, Oct. 2005.

[7] L. A. Farwell and E. Donchin, "Talking off the top of your head: Toward a mental prosthesis utilizing event-related brain potentials," *Electroencephalogr. Clin. Neurophysiol.*, vol. 70, no. 6, pp. 510–523, Apr. 1988.

[8] Y. Xu and Y. Nakajima, "A two-level predictive event-related potential-based brain–computer interface," *IEEE Trans. Biomed. Eng.*, vol. 60, no. 10, pp. 2839–2847, Oct. 2013.

[9] J. D. Bayliss, "Use of the evoked potential P3 component for control in a virtual apartment," *IEEE Trans. Neural Syst. Rehabil. Eng.*, vol. 11, no. 2, pp. 113–116, Jun. 2003.

[10] U. Hoffmann, J. M. Vesin, T. Ebrahimi, and K. Diserens, "An efficient P300-based brain–computer interface for disabled subjects," *J. Neurosci. Methods*, vol. 167, pp. 115–125, Mar. 2008.

[11] T. Liu, L. Goldberg, S. Gao, and B. Hong, "An online brain–computer interface using non-flashing visual evoked potentials," *J. Neural Eng.*, vol. 7, no. 3, pp. 1–9, Apr. 2010.

[12] I. Iturrate, J. M. Antelis, A. Kubler, and J. Minguez, "A noninvasive brain-actuated wheelchair based on a P300 neurophysiological protocol and automated navigation," *IEEE Trans. Robot.*, vol. 25, no. 3, pp. 614–627, Jun. 2009.

[13] Y. Li, J. Pan, F. Wang, and Z. Yu, "A hybrid BCI system combining P300 and SSVEP and its application to wheelchair control," *IEEE Trans. Biomed. Eng.*, vol. 60, no. 11, pp. 3156–3166, Nov. 2013.

[14] K. K. Shyu *et al.*, "Total design of an FPGA-based brain–computer interface control hospital bed nursing system," *IEEE Trans. Ind. Electron.*, vol. 60, no. 7, pp. 2731–2739, Jul. 2013.

[15] M. Palankar *et al.*, "Control of a 9-DoF wheelchair-mounted robotic arm system using a P300 brain computer interface: Initial experiments," in *Proc. Annu. Int. Conf. Rob. Biomimetics*, Feb. 21–26, 2008, pp. 348–353.

[16] C. J. Bell, P. Sheony, R. Chalodhorn, and R. P. Rao, "Control of a humanoid robot by a noninvasive brain–computer interface in humans," *J. Neural Eng.*, vol. 5, no. 2, pp. 214–220, May 2008.

[17] M. Li, W. Li, J. Zhao, Q. Meng, M. Zeng, and G. Chen, "A P300 model for cerebot—A mind-controlled humanoid robot," *Robot Intell. Technol. Appl. 2*, vol. 274, pp. 495–502, 2014.

[18] W. Li, M. Li, and J. Zhao, "Control of humanoid robot via motion-onset visual evoked potentials," *Front Syst. Neurosci.*, vol. 7, pp. 1–11, Jan. 2015.

[19] J. X. Ma, Y. Zhang, A. Cichocki, and F. Matsuno, "A novel EOG/EEG hybrid human–machine interface adopting eye movements and ERPs: Application to robot control," *IEEE Trans. Biomed. Eng.*, vol. 62, no. 3, pp. 876–889, Mar. 2015.

[20] C. L. Fu and K. Chen, "Gait synthesis and sensory control of stair climbing for a humanoid robot," *IEEE Trans. Ind. Electron.*, vol. 55, no. 5, pp. 2111–2119, May 2008.

[21] K. Erbatur and O. Kurt, "Natural ZMP trajectories for biped robot reference generation," *IEEE Trans. Ind. Electron.*, vol. 56, no. 3, pp. 835–845, Mar. 2009.

[22] N. Motoi, T. Suzuki, and K. Ohnishi, "A bipedal locomotion planning based on virtual linear inverted pendulum mode," *IEEE Trans. Ind. Electron.*, vol. 56, no. 1, pp. 54–61, Jan. 2009.

[23] K. Suwanratchatamanee, M. Matsumoto, and S. Hashimoto, "Haptic sensing foot system for humanoid robot and ground recognition with one-leg balance," *IEEE Trans. Ind. Electron.*, vol. 58, no. 8, pp. 3174–3185, Aug. 2011.

[24] A. Balestrino, A. Caiti, and E. Crisostomi, "From remote experiments to web-based learning objects: An advanced telelaboratory for robotics and control systems," *IEEE Trans. Ind. Electron.*, vol. 56, no. 12, pp. 4817–4825, Dec. 2009.

[25] H. Cecotti, A. R. Marathe, and A. J. Ries, "Optimization of single-trial detection of event-related potentials through artificial trials," *IEEE Trans. Biomed. Eng.*, vol. 62, no. 9, pp. 2170–2176, Mar. 2015.

[26] S. Gao, Y. Wang, X. Gao, and B. Hong, "Visual and auditory brain–computer interfaces," *IEEE Trans. Biomed. Eng.*, vol. 61, no. 5, pp. 1436–1447, May 2014.

[27] J. Jin *et al.*, "An adaptive P300-based control system," *J. Neural. Eng.*, vol. 8, no. 3, pp. 1–14, Apr. 2011.

[28] J. Jin, B. Z. Allison, X. Wang, and C. Neuper, "A combined brain–computer interface based on P300 potentials and motion-onset visual evoked potentials," *J. Neurosci. Methods*, vol. 25, no. 2, pp. 265–276, Jan. 2012.

[29] S. Hong, Y. Oh, D. Kim, and B. You, "Real-time walking pattern generation method for humanoid robots by combining feedback," *IEEE Trans. Ind. Electron.*, vol. 61, no. 1, pp. 355–364, Jan. 2014.

[30] S. Y. Shin and C. Kim, "Human-like motion generation and control for humanoid's dual arm object manipulation," *IEEE Trans. Ind. Electron.*, vol. 62, no. 4, pp. 2265–2276, Apr. 2015.

[31] M. Li, W. Li, J. Zhao, Q. Meng, F. Sun, and G. Chen, "An adaptive P300 model for controlling a humanoid robot with mind," in *Proc. IEEE Int. Conf. Rob. Biomimetics (ROBIO)*, Dec. 12–14, 2013, pp. 1390–1395.

[32] M. Li, W. Li, and H. Zhou, "Increasing N200 potentials vial visual stimulus depicting humanoid robot behavior," *Int. J. Neural Syst.*, vol. 26, p. 155039, Nov. 2015.

[33] W. Li, C. Jaramillo, and Y. Li, "A brain computer interface based humanoid robot control system," in *Proc. IASTED Int. Conf. Robot.*, Nov. 7–9, 2011, pp. 390–396.

[34] W. Li, C. Jaramillo, and Y. Li, "Development of mind control system for humanoid robot through a brain computer interface," in *Proc. 2nd Int. Conf. Intell. Syst. Des. Eng. Appl. (ISDEA)*, Jan. 6–7, 2012, pp. 679–682.

[35] J. Zhao, W. Li, and M. Li, "Comparative study of SSVEP- and P300-based models for the telepresence control of humanoid robots," *PLoS One*, vol. 10, pp. 0142168, Nov. 2015.

[36] Y. Renard *et al.*, "OpenViBE: An open-source software platform to design, test and use brain–computer interfaces in real and virtual environments," *Presence (Camb)*, vol. 19, no. 1, pp. 35–53, 2010.

[37] C. Guger, S. Daban, E. Sellers, C. Holzner, G. Krausz, and R. Carabalona, "How many people are able to control a P300-based brain–computer interface (BCI)?" *Neurosci. Lett.*, vol. 462, no. 1, pp. 94–98, Jun. 2009.

[38] D. J. Krusienski, E. W. Sellers, D. J. McFarland, T. M. Vaughan, and J. R. Wolpaw, "Toward enhanced P300 speller performance," *J. Neurosci. Methods*, vol. 167, pp. 15–21, Jan. 2008.
[39] S. Mika, G. Ratsch, J. Weston, B. Scholkopf, and K. R. Mullers, "Fisher discriminant analysis with kernels," in *Proc. IEEE Signal Process. Soc. Workshop, Neural Netw. Signal Process. IX*, Aug. 23–25, 1999, pp. 41–48.
[40] A. Rakotomamonjy and V. Guigue, "BCI competition III: Dataset II-ensemble of SVMs for BCI P300 speller," *IEEE Trans. Biomed. Eng.*, vol. 55, no. 3, pp. 1147–1154, Mar. 2008.
[41] C. Juang and G. Chen, "A TS fuzzy system learned through a support vector machine in principal component space for real-time object detection," *IEEE Trans. Ind. Electron.*, vol. 59, no. 8, pp. 3309–3320, Aug. 2012.
[42] C. C. Chang and C. J. Lin, "LIBSVM: A library for support vector machine," *ACM Trans. Intell. Syst. Technol.*, vol. 2, no. 3, pp. 1–39, 2011.
[43] A. Subasi and M. I. Gursoy, "EEG signal classification using PCA, ICA, LDA and support vector machines," *Exp. Syst. Appl.*, vol. 37, pp. 8659–8666, Dec. 2010.

Mengfan Li received the B.E. degree in automation from Hebei University of Technology, Tianjin, China, in 2011. She is currently working toward the Ph.D. degree in electrical engineering and automation at Tianjin University, Tianjin, China.

Her research interests include event-related potentials and brain–robot interaction.

Wei Li (M'94) received the B.S. and M.S. degrees in electrical engineering from Northern Jiaotong University, Beijing, China, in 1982 and 1984, respectively, and the Ph.D. degree in electrical and computer engineering from the University of Saarland, Saarbrücken, Germany, in 1991.

He has been appointed a Guest Professor with the State Key Laboratory of Robotics, Shenyang Institute of Automation, Chinese Academy of Sciences, Shenyang, China, and an Adjunct Professor with the School of Electrical Engineering and Automation, Tianjin University, Tianjin, China. He was an Alexander von Humboldt Foundation Research Fellow with the Technical University of Braunschweig, Braunschweig, Germany, from 1997 to 1999. He was a Full Professor of Computer Science and Technology with Tsinghua University, Beijing, China. He is currently a Professor with the Department of Computer and Electrical Engineering and Computer Science, California State University, Bakersfield, CA, USA. His research interests include brain–robot interaction, biologically inspired robots, chemical plume tracing and mapping, fuzzy control and modeling, and multisensor fusion and integration.

Linwei Niu (M'05) received the B.S. degree in computer science and technology from Peking University, Beijing, China, in 1998, the M.S. degree in computer science from the State University of New York at Stony Brook, Stony Brook, NY, USA, in 2001, and the Ph.D. degree in computer science and engineering from the University of South Carolina, Columbia, SC, USA, in 2006.

He is currently an Associate Professor with the Department of Mathematics and Computer Science, West Virginia State University, Institute, WV, USA. His research interests include power-aware design for embedded systems, design automation, real-time scheduling, and software/hardware codesign.

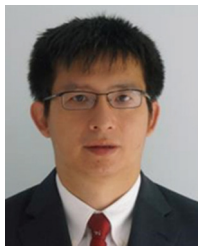

Huihui Zhou received the B.E. degree in biomedical engineering from Zhejiang University, Hangzhou, China, in 1995, and the Ph.D. degree in physiology from the Chinese Academy of Medical Sciences and Peking Union Medical College, Beijing, China, in 2000.

He is currently a Professor with the Shenzhen Institutes of Advanced Technology (SIAT), Chinese Academy of Sciences, Shenzhen, China. His research interests include visual cognition and behavior, attention and eye movement, neural signal processing, and brain–machine interface.

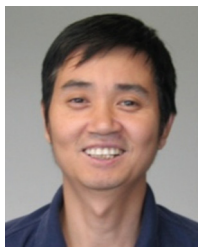

Genshe Chen (M'05) received the B.S. and M.S. degrees in electrical engineering in 1989 and 1991, respectively, and the Ph.D. degree in aerospace engineering in 1994, all from Northwestern Polytechnical University, Xi'an, China.

He was with the Institute of Flight Guidance and Control, Technical University of Braunschweig, Braunschweig, Germany, and with the Flight Division of National Aerospace Laboratory of Japan, Mitika, Tokyo, Japan, from 1997 to 2001. He was the Chief Technology Officer (CTO) of DCM Research Resources LLC, Germantown, MD, USA, and the Program Manager of Networks, Systems and Control, Intelligent Automation, Inc., Rockville, MD, USA. He is currently the Chief Technological Officer of Intelligent Fusion Technology, Inc., Germantown, MD, USA. His research interests include SWAP-C sensor design, intelligent signal processing, multi-INT fusion, space situational awareness, cognitive radio for satellite communication, cooperative control and optimization for military operations, guidance, navigation, and control, cyber security, C4ISR, electronic warfare, game theory, graphical theory, and human–cyber–physical systems.

Feng Duan received the B.S. and M.S. degrees in mechanical engineering from Tianjin University, Tianjin, China, in 2002 and 2004, respectively, and the M.S. and Ph.D. degrees in precision engineering from The University of Tokyo, Tokyo, Japan, in 2006 and 2009, respectively.

He is currently an Associate Professor with Nankai University, Tianjin, China. His research interests include cellular manufacture systems, rehabilitation robots, and brain–machine interfaces.

Dr. Duan was the recipient of the Award of the Japanese Society for Artificial Intelligence (for the proposal of the standard platform in a home league 2014), the FANUC FA Robot Foundation Best Paper Award (2011), the Chinese Government Award for Outstanding Self-Financed Students Abroad (2008), the IEEE Conference on Automation Science and Engineering Best Student Paper Award (2008), and a winner of RoboCup @Home Simulation in the RoboCup Japan Open (First Runner-Up 2014).